Original Research Article: full paper

(2024), «EUREKA: Physics and Engineering»
Number 4

MODELING OF MILLING FORCES IN FACING PROCESS OF ALUMINUM ALLOY Al7075 USING THE SQUARE INSERTS

Nhu-Tung Nguyen✉
International School[1]
tungnn@vnuis.edu.vn

Hai Xuan Le
International School[1]

Thinh Xuan Hoang
School of Mechanical and Automotive Engineering
Hanoi University of Industry
298 Cau Dien str., Bac Tu Liem District, Hanoi, Vietnam, 11915

Van-Hai Nguyen
Faculty of Mechanical Engineering and Mechatronics
PHENIKAA University
Yen Nghia Ward, Ha Dong District, Hanoi, Vietnam, 12116

Huu-Hung Nguyen
Faculty of Natural Sciences (FNS)
Hung Vuong University
Nong Trang Ward, Viet Tri, Phu Tho Province, Vietnam, 290000

[1]*Vietnam National University*
144 Xuan Thuy str., Hanoi city, Vietnam, 11310

✉**Corresponding author**

Abstract

Cutting forces play very important in designing the tool machine, cutting tool, and in optimization of machining processes. Modeling and prediction of cutting forces by theoretical methods are quite difficult, so, this study was focused on modeling the cutting force in face milling process using combination of theoretical and experimental methods. This study was performed to model the milling forces (MFs) and determine the milling force coefficients (MFCs) in the face milling process of aluminum alloy Al7075 using square inserts. From theoretical and experimental methods, the relationship of average milling forces (AMFs) and feed per flute (ft) were determined as the linear regression. Using experimental data, the linear regressions of AMFs and feed per flute were determined with high values of determination coefficients (larger than 95 %). MFCs were determined including shear and edge MFCs (tangential shear MFC (K_{tc}) of 538.127 N/mm^2, radial shear MFC (K_{rc}) of 185.967 N/mm^2, axial shear MFC (K_{ac}) of –691.297 N/mm^2, tangential edge MFC (K_{te}) of 11.253 N/mm, radial edge MFC (K_{re}) of 6.991 N/mm, and axial edge MFC (K_{ae}) of –32.971 N/mm. The MF models were successfully verified by comparing the measured and predicted MFs in face milling process of Al7075. The tendency and shape of predicted MFs were quite close to the measured ones. The differences between the predicted and the measured MFs can be due to the several reasons such as the influence of vibrations, the influence of cutting heat, etc., and these are also the limitations of this study. The modeling and prediction methods of this study can be used to model and predict the cutting forces in face milling of other milling types and other pairs of cutting tool and workpiece material as well.

Keywords: modelling, MFs, MFCs, AMF, shear milling force, edge milling force, square inserts, prediction, aluminum alloy, Al7075.

DOI: 10.21303/2461-4262.2024.003209

1. Introduction

Many studies were performed to model the MFs and to determine the MFCs [1–3]. MFs can be modeled from simple cutting processes [4], complex cutting processes [5] with different approaches such as theoretical modeling [6] or experimental modeling [7]. The theoretical models

are often very difficult to build because almost all parameters must be built based on physical, geometric, and mechanical phenomena. The experimental model can give quick prediction results. However, the predicted results are only representative values, not detailed values for the entire machining process. In addition, the experimental model can only be applied to each specific case and cannot be applied generally to many different cases.

The MF models are built for common types of milling methods like machining with complex geometrical cutters [8]. Many studies were performed to model the MFs and predict the MFCs for the milling processes using flat-end mills [1], using ball-end mills [9], using parallelogram inserts [9], and so on. Applying the experimental method, the cutting forces were predicted in face milling processes using round inserts [10, 11]. However, modeling of MFs and determination of MFCs for some types of face milling using square inserts has not been mentioned.

With the milling process using a flat-end mill cutter, ball-end mill cutter, or using parallelogram inserts, the previous studies showed that, by both theoretical modeling and experimental modeling, the average cutting forces (ACFs) can always be expressed as a linear function of the feed per flute (ft) [9]. This study was conducted to build the milling force models and determine the milling force coefficients by combining both theoretical and experimental methods in the face milling process of Al7075 alloy using square inserts.

There are two main sections of this study including the theoretical modeling section and the experimental one. In the first section, according to the geometrical, mechanical, physical phenomena, the milling forces were modeled as the functions of cutter geometry parameters, cutting parameters, and the milling force coefficients. By theoretical method, the equations that were applied to calculate the cutting force coefficients were also built based on the cutter parameters, cutting parameters. In the second section, the milling force coefficients were determined using the experimental data of milling forces. Besides, the milling force models were also verified by comparing the predicted of milling forces with measured ones.

2. Materials and methods

2. 1. Theoretical modeling of milling forces in facing process using the square inserts

In the facing process, the components of the cutting process include cutter and workpiece (**Fig. 1, *a***), the shape and size of the cutting insert will determine the size and shape of the formed chip as described in **Fig. 1, *b***.

The cutter rotation angle (ϕ_j) and the point position at z coordinate of cutting edge are calculated by (1) and described in **Fig. 1, *b*, *c***, [9]:

$$\begin{cases} \phi_j = \phi_1 + \phi_j(j-1), \quad j = 1 \div N; \\ \phi_j(z) = \phi_j - \psi = \phi_j - \dfrac{\tan\beta}{R}, \end{cases} \tag{1}$$

where ψ – the lag angle and β is the helix angle in milling process as shown in **Fig. 1**.

In face milling process, based on the cutter and workpiece interaction (**Fig. 2, *a***), The thickness of undeform chip and length of cutting edge were described in **Fig. 2, *b*** and calculated by (2):

$$\begin{cases} h_j\left(\phi_j(z)\right) = f_t * \sin\left(\phi_1(z)\right) * \sin\left(\kappa(z)\right); \\ ds = dz * \sqrt{\dfrac{(r-z)^2}{r^2-(r-z)^2} + \left(\dfrac{R+\sqrt{r^2-(r-z)^2}}{R}\right)^2} * \tan^2\beta = \Lambda * dz. \end{cases} \tag{2}$$

For each cutting edge element, the CF components (**Fig. 2, *c***) are calculated by (3) [9]:

$$\begin{cases} dF_{t,j}(\phi,z) = \left(\sin(\phi_j(z)) * K_{tc} * f_t + \Lambda * K_{te}\right)dz; \\ dF_{r,j}(\phi,z) = \left(\sin(\phi_j(z)) * K_{tr} * f_t + \Lambda * K_{re}\right)dz; \\ dF_{a,j}(\phi,z) = \left(\sin(\phi_j(z)) * K_{ac} * f_t + \Lambda * K_{ae}\right)dz, \end{cases} \tag{3}$$

where K_{tc}, K_{rc}, K_{ac}, K_{te}, K_{re} – milling force coefficients (MFCs).

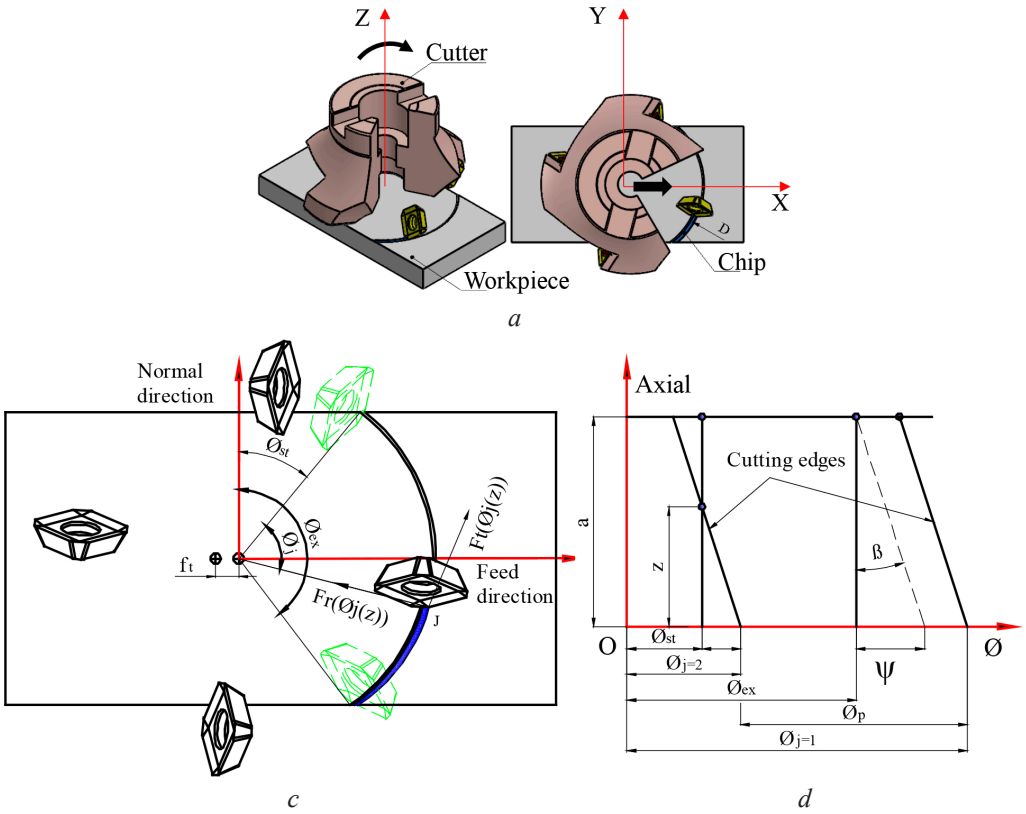

Fig. 1. Face milling model using square inserts: *a* – milling components; *b* – cutter positions in top view; *c* – cutting edge positions with helix angle

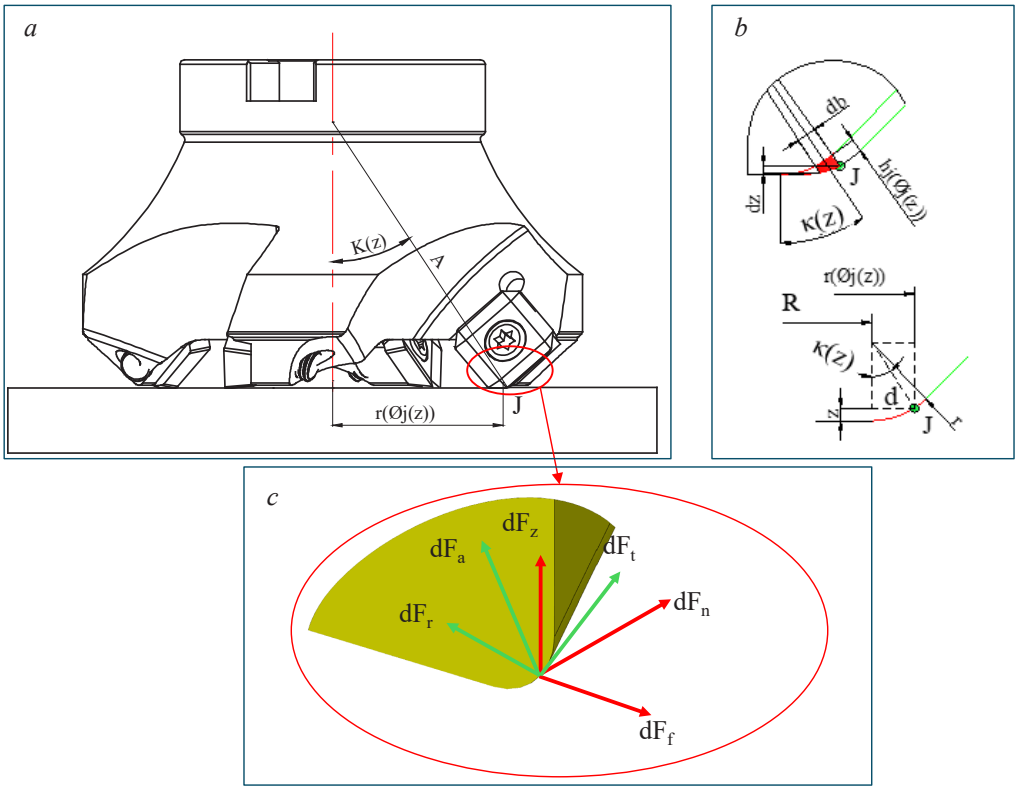

Fig. 2. MF in face milling process: *a* – cutter and workpiece interaction; *b* – thickness and length of cutting edge; *c* – MF components

The differential milling force at each cutting point can be calculated by (4) and (5):

$$\begin{Bmatrix} dF_{\mathrm{f},j}(\phi,z) \\ dF_{\mathrm{n},j}(\phi,z) \\ dF_{a,j}(\phi,z) \end{Bmatrix} = \begin{bmatrix} -\cos(\phi_j(z)) & -\sin(\kappa(z))*\sin(\phi_j(z)) & -\cos(\kappa(z))*\sin(\phi_j(z)) \\ \sin(\phi_j(z)) & -\sin(\kappa(z))*\cos(\phi_j(z)) & -\cos(\kappa(z))*\sin(\phi_j(z)) \\ 0 & \cos(\kappa(z)) & -\sin(\kappa(z)) \end{bmatrix} \begin{Bmatrix} dF_{t,j}(\phi,z) \\ dF_{r,j}(\phi,z) \\ dF_{a,j}(\phi,z) \end{Bmatrix}, \quad (4)$$

$$\begin{cases} dF_{f,j}(\phi,z) = \cos\left(\phi_j - \dfrac{\tan\beta}{R}z\right)*dF_{t,j}(\phi,z) + \sin\left(\phi_j - \dfrac{\tan\beta}{R}z\right)*\sin(\kappa(z))*dF_{r,j}(\phi,z) + \\ \qquad + \sin\left(\phi_j - \dfrac{\tan\beta}{R}z\right)*\cos(\kappa(z))*dF_{a,j}(\phi,z); \\ dF_{n,j}(\phi,z) = \cos\left(\phi_j - \dfrac{\tan\beta}{R}z\right)*dF_{t,j}(\phi,z) + \sin\left(\phi_j - \dfrac{\tan\beta}{R}z\right)*\sin(\kappa(z))*dF_{r,j}(\phi,z) + \\ \qquad + \sin\left(\phi_j - \dfrac{\tan\beta}{R}z\right)*\cos(\kappa(z))*dF_{a,j}(\phi,z); \\ dF_{a,j}(\phi,z) = \cos\left(\phi_j - \dfrac{\tan\beta}{R}z\right)*dF_{t,j}(\phi,z) + \sin\left(\phi_j - \dfrac{\tan\beta}{R}z\right)*\sin(\kappa(z))*dF_{r,j}(\phi,z) + \\ \qquad + \sin\left(\phi_j - \dfrac{\tan\beta}{R}z\right)*\cos(\kappa(z))*dF_{a,j}(\phi,z). \end{cases} \quad (5)$$

In (4) and (5), the MFCs can be calculated by (6):

$$\begin{cases} K_{ac} = \dfrac{(C_3C_7C_{15} - C_1C_9C_{15})\overline{F}_{ac} - C_7C_{13}C_{15}\overline{F}_{fc} + C_1C_{13}C_{15}\overline{F}_{nc}}{C_3C_7C_{15}^2 - C_5C_7C_{13}C_{15} - C_1C_9C_{15}^2 + C_1C_{11}C_{13}C_{15}}; \\ K_{ae} = \dfrac{(C_4C_8C_{16} - C_2C_{10}C_{16})\overline{F}_{ae} - C_8C_{14}C_{16}\overline{F}_{fe} + C_2C_{14}C_{16}\overline{F}_{ne}}{C_4C_8C_{16}^2 - C_8C_8C_{14}C_{16} - C_2C_{10}C_{16}^2 + C_2C_{12}C_{14}C_{16}}; \\ K_{rc} = \dfrac{(C_1C_{11} - C_5C_7)\overline{F}_{ac} + C_7C_{15}\overline{F}_{fc} - C_1C_{15}\overline{F}_{nc}}{C_3C_7C_{15} - C_5C_7C_{13} - C_1C_9C_{15} + C_1C_{11}C_{13}}; \\ K_{re} = \dfrac{(C_2C_{12} - C_6C_8)\overline{F}_{ae} + C_8C_{16}\overline{F}_{fc} - C_2C_{16}\overline{F}_{ne}}{C_4C_8C_{16} - C_6C_8C_{14} - C_2C_{10}C_{16} + C_2C_{12}C_{14}}; \\ K_{tc} = \dfrac{\overline{F}_{fc} - C_3\overline{F}_{rc} - C_5\overline{F}_{ac}}{C_1}; \\ K_{te} = \dfrac{\overline{F}_{fe} - C_4\overline{F}_{re} - C_6\overline{F}_{ae}}{C_2}. \end{cases} \quad (6)$$

In (6), the linear components ($\overline{F}_{fc}$, $\overline{F}_{fe}$, $\overline{F}_{nc}$, $\overline{F}_{ne}$, $\overline{F}_{ac}$, and $\overline{F}_{ae}$) are determined depending on the linear relationship of average MFs and feed per flute. These values can be determined based on the milling experimental data of average MFs. The constants (C_1 to C_{16}) are determined based on the cutter geometry and the cutting condition parameters and can be calculated by (7) to (22):

$$C_1 = -\frac{N}{4\pi}\left[\int_{\phi_{st}}^{\phi_{st}+\psi}\left(\int_0^{\frac{R}{\tan\beta}(\phi_j-\phi_{st})}\sin 2\left(\phi_j - \frac{\tan\beta}{R}z\right)dz\right)d\phi + \int_{\phi_{st}+\psi}^{\phi_{ex}}\left(\int_0^{a}\sin 2\left(\phi_j - \frac{\tan\beta}{R}z\right)dz\right)d\phi + \right.$$
$$\left. + \int_{\phi_{ex}}^{\phi_{ex}+\psi}\left(\int_{\frac{R}{\tan\beta}(\phi_j-\phi_{ex})}^{a}\sin 2\left(\phi_j - \frac{\tan\beta}{R}z\right)dz\right)d\phi\right], \quad (7)$$

$$C_2 = -\frac{N}{2\pi}\left[\begin{array}{l}\int\limits_{\phi_{st}}^{\phi_{st}+\psi}\left(\int\limits_{0}^{\frac{R}{\tan\beta}(\phi_j-\phi_{st})}\Lambda * \cos\left(\phi_j - \frac{\tan\beta}{R}z\right)dz\right)d\phi + \int\limits_{\phi_{st}+\psi}^{\phi_{ex}}\left(\int\limits_{0}^{a}\Lambda * \cos\left(\phi_j - \frac{\tan\beta}{R}z\right)dz\right)d\phi + \\ + \int\limits_{\phi_{ex}}^{\phi_{ex}+\psi}\left(\int\limits_{\frac{R}{\tan\beta}(\phi_j-\phi_{ex})}^{a}\Lambda * \cos\left(\phi_j - \frac{\tan\beta}{R}z\right)dz\right)d\phi\end{array}\right], \quad (8)$$

$$C_3 = -\frac{N}{4\pi}\left[\begin{array}{l}\int\limits_{\phi_{st}}^{\phi_{st}+\psi}\left(\int\limits_{0}^{\frac{R}{\tan\beta}(\phi_j-\phi_{st})}\sin(\kappa(z)) * \left(1-\cos 2\left(\phi_j - \frac{\tan\beta}{R}z\right)\right)dz\right)d\phi + \\ + \int\limits_{\phi_{st}+\psi}^{\phi_{ex}}\left(\int\limits_{0}^{a}\sin(\kappa(z)) * \left(1-\cos 2\left(\phi_j - \frac{\tan\beta}{R}z\right)\right)dz\right)d\phi + \\ + \int\limits_{\phi_{ex}}^{\phi_{ex}+\psi}\left(\int\limits_{\frac{R}{\tan\beta}(\phi_j-\phi_{ex})}^{a}\sin(\kappa(z)) * \left(1-\cos 2\left(\phi_j - \frac{\tan\beta}{R}z\right)\right)dz\right)d\phi\end{array}\right], \quad (9)$$

$$C_4 = -\frac{N}{2\pi}\left[\begin{array}{l}\int\limits_{\phi_{st}}^{\phi_{st}+\psi}\left(\int\limits_{0}^{\frac{R}{\tan\beta}(\phi_j-\phi_{st})}\Lambda * \sin(\kappa(z)) * \sin\left(\phi_j - \frac{\tan\beta}{R}z\right)dz\right)d\phi + \\ + \int\limits_{\phi_{st}+\psi}^{\phi_{ex}}\left(\int\limits_{0}^{a}\Lambda * \sin(\kappa(z)) * \sin\left(\phi_j - \frac{\tan\beta}{R}z\right)dz\right)d\phi + \\ + \int\limits_{\phi_{ex}}^{\phi_{ex}+\psi}\left(\int\limits_{\frac{R}{\tan\beta}(\phi_j-\phi_{ex})}^{a}\Lambda * \sin(\kappa(z)) * \sin\left(\phi_j - \frac{\tan\beta}{R}z\right)dz\right)d\phi\end{array}\right], \quad (10)$$

$$C_5 = -\frac{N}{4\pi}\left[\begin{array}{l}\int\limits_{\phi_{st}}^{\phi_{st}+\psi}\left(\int\limits_{0}^{\frac{R}{\tan\beta}(\phi_j-\phi_{st})}\cos(\kappa(z)) * \left(1-\cos 2\left(\phi_j - \frac{\tan\beta}{R}z\right)\right)dz\right)d\phi + \\ + \int\limits_{\phi_{st}+\psi}^{\phi_{ex}}\left(\int\limits_{0}^{a}\cos(\kappa(z)) * \left(1-\cos 2\left(\phi_j - \frac{\tan\beta}{R}z\right)\right)dz\right)d\phi + \\ + \int\limits_{\phi_{ex}}^{\phi_{ex}+\psi}\left(\int\limits_{\frac{R}{\tan\beta}(\phi_j-\phi_{ex})}^{a}\cos(\kappa(z)) * \left(1-\cos 2\left(\phi_j - \frac{\tan\beta}{R}z\right)\right)dz\right)d\phi\end{array}\right], \quad (11)$$

$$C_6 = -\frac{N}{2\pi}\left[\begin{array}{l}\int\limits_{\phi_{st}}^{\phi_{st}+\psi}\left(\int\limits_{0}^{\frac{R}{\tan\beta}(\phi_j-\phi_{st})}\Lambda * \cos(\kappa(z))\sin\left(\phi_j - \frac{\tan\beta}{R}z\right)dz\right)d\phi + \\ + \int\limits_{\phi_{st}+\psi}^{\phi_{ex}}\left(\int\limits_{0}^{a}\Lambda * \cos(\kappa(z))\sin\left(\phi_j - \frac{\tan\beta}{R}z\right)dz\right)d\phi + \\ + \int\limits_{\phi_{ex}}^{\phi_{ex}+\psi}\left(\int\limits_{\frac{R}{\tan\beta}(\phi_j-\phi_{ex})}^{a}\Lambda * \cos(\kappa(z))\sin\left(\phi_j - \frac{\tan\beta}{R}z\right)dz\right)d\phi\end{array}\right], \quad (12)$$

$$C_7 = \frac{N}{4\pi}\left[\begin{array}{l}\int\limits_{\phi_{st}}^{\phi_{st}+\psi}\left(\int\limits_{0}^{\frac{R}{\tan\beta}(\phi_j-\phi_{st})}\left(1-\cos 2\left(\phi_j-\frac{\tan\beta}{R}z\right)\right)dz\right)d\phi+\\ +\int\limits_{\phi_{st}+\psi}^{\phi_{ex}}\left(\int\limits_{0}^{a}\left(1-\cos 2\left(\phi_j-\frac{\tan\beta}{R}z\right)\right)dz\right)d\phi+\\ +\int\limits_{\phi_{ex}}^{\phi_{ex}+\psi}\left(\int\limits_{\frac{R}{\tan\beta}(\phi_j-\phi_{ex})}^{a}\left(1-\cos 2\left(\phi_j-\frac{\tan\beta}{R}z\right)\right)dz\right)d\phi\end{array}\right], \quad (13)$$

$$C_8 = \frac{N}{2\pi}\left[\begin{array}{l}\int\limits_{\phi_{st}}^{\phi_{st}+\psi}\left(\int\limits_{0}^{\frac{R}{\tan\beta}(\phi_j-\phi_{st})}\Lambda*\sin\left(\phi_j-\frac{\tan\beta}{R}z\right)dz\right)d\phi+\\ +\int\limits_{\phi_{st}+\psi}^{\phi_{ex}}\left(\int\limits_{0}^{a}\Lambda*\sin\left(\phi_j-\frac{\tan\beta}{R}z\right)dz\right)d\phi+\\ +\int\limits_{\phi_{ex}}^{\phi_{ex}+\psi}\left(\int\limits_{\frac{R}{\tan\beta}(\phi_j-\phi_{ex})}^{a}\Lambda*\sin\left(\phi_j-\frac{\tan\beta}{R}z\right)dz\right)d\phi\end{array}\right], \quad (14)$$

$$C_9 = -\frac{N}{4\pi}\left[\begin{array}{l}\int\limits_{\phi_{st}}^{\phi_{st}+\psi}\left(\int\limits_{0}^{\frac{R}{\tan\beta}(\phi_j-\phi_{st})}\sin(\kappa(z))*\sin 2\left(\phi_j-\frac{\tan\beta}{R}z\right)dz\right)d\phi+\\ +\int\limits_{\phi_{st}+\psi}^{\phi_{ex}}\left(\int\limits_{0}^{a}\sin(\kappa(z))*\sin 2\left(\phi_j-\frac{\tan\beta}{R}z\right)dz\right)d\phi+\\ +\int\limits_{\phi_{ex}}^{\phi_{ex}+\psi}\left(\int\limits_{\frac{R}{\tan\beta}(\phi_j-\phi_{ex})}^{a}\sin(\kappa(z))*\sin 2\left(\phi_j-\frac{\tan\beta}{R}z\right)dz\right)d\phi\end{array}\right], \quad (15)$$

$$C_{10} = -\frac{N}{2\pi}\left[\begin{array}{l}\int\limits_{\phi_{st}}^{\phi_{st}+\psi}\left(\int\limits_{0}^{\frac{R}{\tan\beta}(\phi_j-\phi_{st})}\Lambda*\sin(\kappa(z))*\cos\left(\phi_j-\frac{\tan\beta}{R}z\right)dz\right)d\phi+\\ +\int\limits_{\phi_{st}+\psi}^{\phi_{ex}}\left(\int\limits_{0}^{a}\Lambda*\sin(\kappa(z))*\cos\left(\phi_j-\frac{\tan\beta}{R}z\right)dz\right)d\phi+\\ +\int\limits_{\phi_{ex}}^{\phi_{ex}+\psi}\left(\int\limits_{\frac{R}{\tan\beta}(\phi_j-\phi_{ex})}^{a}\Lambda*\sin(\kappa(z))*\cos\left(\phi_j-\frac{\tan\beta}{R}z\right)dz\right)d\phi\end{array}\right], \quad (16)$$

$$C_{11} = -\frac{N}{4\pi}\left[\begin{array}{l}\int\limits_{\phi_{st}}^{\phi_{st}+\psi}\left(\int\limits_{0}^{\frac{R}{\tan\beta}(\phi_j-\phi_{st})}\cos(\kappa(z))*\sin 2\left(\phi_j-\frac{\tan\beta}{R}z\right)dz\right)d\phi+\\ +\int\limits_{\phi_{st}+\psi}^{\phi_{ex}}\left(\int\limits_{0}^{a}\cos(\kappa(z))*\sin 2\left(\phi_j-\frac{\tan\beta}{R}z\right)dz\right)d\phi+\\ +\int\limits_{\phi_{ex}}^{\phi_{ex}+\psi}\left(\int\limits_{\frac{R}{\tan\beta}(\phi_j-\phi_{ex})}^{a}\cos(\kappa(z))*\sin 2\left(\phi_j-\frac{\tan\beta}{R}z\right)dz\right)d\phi\end{array}\right], \quad (17)$$

$$C_{12}=-\frac{N}{2\pi}\left[\begin{array}{l}\int\limits_{\phi_{st}}^{\phi_{st}+\psi}\left(\int\limits_{0}^{\frac{R}{\tan\beta}(\phi_j-\phi_{st})}\Lambda*\cos(\kappa(z))*\cos\left(\phi_j-\frac{\tan\beta}{R}z\right)dz\right)d\phi+\\ +\int\limits_{\phi_{st}+\psi}^{\phi_{ex}}\left(\int\limits_{0}^{a}\Lambda*\cos(\kappa(z))*\cos\left(\phi_j-\frac{\tan\beta}{R}z\right)dz\right)d\phi+\\ +\int\limits_{\phi_{ex}}^{\phi_{ex}+\psi}\left(\int\limits_{\frac{R}{\tan\beta}(\phi_j-\phi_{ex})}^{a}\Lambda*\cos(\kappa(z))*\cos\left(\phi_j-\frac{\tan\beta}{R}z\right)dz\right)d\phi\end{array}\right], \quad (18)$$

$$C_{13}=\frac{N}{2\pi}\left[\begin{array}{l}\int\limits_{\phi_{st}}^{\phi_{st}+\psi}\left(\int\limits_{0}^{\frac{R}{\tan\beta}(\phi_j-\phi_{st})}\sin\left(\phi_j-\frac{\tan\beta}{R}z\right)*\cos(\kappa(z))dz\right)d\phi+\\ +\int\limits_{\phi_{st}+\psi}^{\phi_{ex}}\left(\int\limits_{0}^{a}\sin\left(\phi_j-\frac{\tan\beta}{R}z\right)*\cos(\kappa(z))dz\right)d\phi+\\ +\int\limits_{\phi_{ex}}^{\phi_{ex}+\psi}\left(\int\limits_{\frac{R}{\tan\beta}(\phi_j-\phi_{ex})}^{a}\sin\left(\phi_j-\frac{\tan\beta}{R}z\right)*\cos(\kappa(z))dz\right)d\phi\end{array}\right], \quad (19)$$

$$C_{14}=\frac{N}{2\pi}\left[\begin{array}{l}\int\limits_{\phi_{st}}^{\phi_{st}+\psi}\left(\int\limits_{0}^{\frac{R}{\tan\beta}(\phi_j-\phi_{st})}\left(\Lambda*\cos(\kappa(z))\right)dz\right)d\phi+\int\limits_{\phi_{st}+\psi}^{\phi_{ex}}\left(\int\limits_{0}^{a}\left(\Lambda*\cos(\kappa(z))\right)dz\right)d\phi+\\ +\int\limits_{\phi_{ex}}^{\phi_{ex}+\psi}\left(\int\limits_{\frac{R}{\tan\beta}(\phi_j-\phi_{ex})}^{a}\left(\Lambda*\cos(\kappa(z))\right)dz\right)d\phi\end{array}\right], \quad (20)$$

$$C_{15}=-\frac{N}{2\pi}\left[\begin{array}{l}\int\limits_{\phi_{st}}^{\phi_{st}+\psi}\left(\int\limits_{0}^{\frac{R}{\tan\beta}(\phi_j-\phi_{st})}\left(\sin(\kappa(z))*\sin\left(\phi_j-\frac{\tan\beta}{R}z\right)\right)dz\right)d\phi+\\ +\int\limits_{\phi_{st}+\psi}^{\phi_{ex}}\left(\int\limits_{0}^{a}\left(\sin(\kappa(z))*\sin\left(\phi_j-\frac{\tan\beta}{R}z\right)\right)dz\right)d\phi+\\ +\int\limits_{\phi_{ex}}^{\phi_{ex}+\psi}\left(\int\limits_{\frac{R}{\tan\beta}(\phi_j-\phi_{ex})}^{a}\left(\sin(\kappa(z))*\sin\left(\phi_j-\frac{\tan\beta}{R}z\right)\right)dz\right)d\phi\end{array}\right], \quad (21)$$

$$C_{16}=-\frac{N}{2\pi}\left[\begin{array}{l}\int\limits_{\phi_{st}}^{\phi_{st}+\psi}\left(\int\limits_{0}^{\frac{R}{\tan\beta}(\phi_j-\phi_{st})}\left(\sin(\kappa(z))*\Lambda\right)dz\right)d\phi+\int\limits_{\phi_{st}+\psi}^{\phi_{ex}}\left(\int\limits_{0}^{a}\left(\sin(\kappa(z))*\Lambda\right)dz\right)d\phi+\\ +\int\limits_{\phi_{ex}}^{\phi_{ex}+\psi}\left(\int\limits_{\frac{R}{\tan\beta}(\phi_j-\phi_{ex})}^{a}\left(\sin(\kappa(z))*\Lambda\right)dz\right)d\phi\end{array}\right], \quad (22)$$

where ϕ_{st} – the start angle in milling processes and ϕ_{ex} – the exit angle in milling processes.

2. 2. Experimental method

A 5-axis CNC milling machine was used during the experimental processes with the following parameters: model: DMU 50 ECOLINE, the control system: SINUMERIK S840DSB, the table size: 500×630 mm, the *X*-axis travel: 500 mm, the *Y*-axis travel: 450 mm, the *Z*-axis travel: 400 mm, and the maximum spindle speed: 10000 rpm. The experimental machine is shown in **Fig. 3.**

Fig. 3. Five-axis CNC milling machine

The dimensions of workpiece are 80×40×28 mm as shown in **Fig. 4**. The compositions of Al7075 alloy are listed in **Table 1**. The main several properties of this workpiece material were hardness of 60 HB, Young's modulus of 70–80 GPa, density of 2.7 g/cm^3.

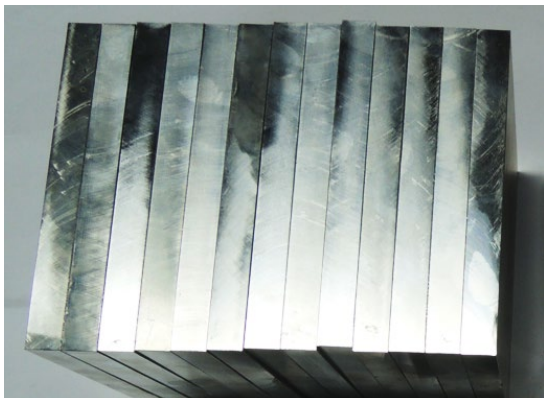

Fig. 4. Experimental workpieces

Table 1

Composites of Al7075 alloy

Composition	Cu	Mn	Mg	Cr	Zn	Ti	Al
%	1.2–2.0	0.3	2.1–2.9	0.18–0.28	5.1–6.1	0.2	remains

A cutter with diameter of 63 mm and with four Carbide square inserts (SEET13T3-HO-ECM100, ECHAIN-TAIWAN) was used in the face milling process. The insert noise radius of inserts was 0.4 mm ($r = 0.4$ mm). The cutter helix angle was 30 degrees. The tool holder and inserts were described in **Fig. 5**.

The dynamometer system (type Kistler 9139AA) from the Kisler company (Swiss) was used to measure the three components of cutting forces (F_x, F_y, F_z) in face milling processes as shown in **Fig. 6**. The force measurement ranges of this system are from –3 KN to 3 KN. The data acquisition and processing system (type 3160-B-042) with the computer and DynoWare software was used to collect and analyze the cutting force data in experimental processes.

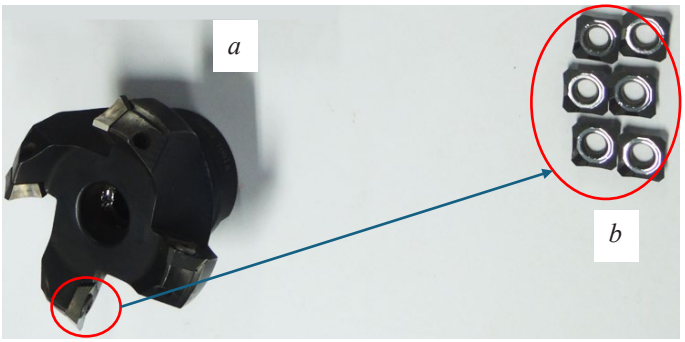

Fig. 5. Milling holder and inserts: *a* – milling holder; *b* – inserts

a *b*

Fig. 6. Experimental system:
a – cutting process components; *b* – signal collecting and processing

The experiments were selected with the constants of axial depth of cut (*a*), constants of radial width of cut (*b*), constants of spindle speed (*n*), and with the variation of feed per flute (*ft*) to determine the average milling force-feed rate relationship and to verify the MFMs as listed in **Table 2**.

Table 2
Experimental plan

No.	Cutter parameters				Cutting parameters			
	D **(mm)**	***N*** **(teeth)**	***r*** **(mm)**	**β (°)**	***a*** **(mm)**	***b*** **(mm)**	***f*** **(mm/tooth)**	***n*** **(rpm)**
1	63	4	0.4	30	0.4	28	0.10	1000
2	63	4	0.4	30	0.4	28	0.15	1000
3	63	4	0.4	30	0.4	28	0.20	1000
4	63	4	0.4	30	0.4	28	0.25	1000
5	63	4	0.4	30	0.4	28	0.30	1000

3. Results and Discussion

3. 1. Average milling forces (AMFs) and feed per flute (ft) relationship

Average MFs and feed per flute relationship was built in **Fig. 7.** It is clear that in all directions, AMF-*ft* relationship was a linear function with high determination coefficients (larger than 95 %). Besides, in all three directions, if the *ft* increases, the absolute values of AMFs also increase.

Equation (6) was used to determine six MFCs and listed in **Table 3**. It is clear that the shear MFCs were the most important MFCs, because the absolute values of shear MFCs are larger more times than the absolute values of edge MFCs.

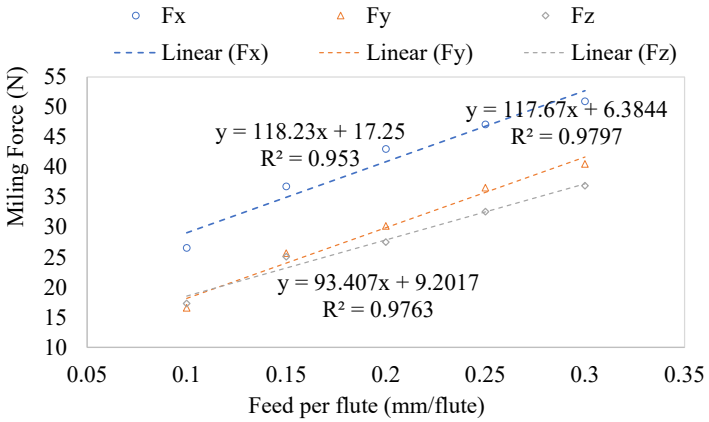

Fig. 7. ACF-*ft* relationship

Table 3
Shear and edge MFCs

Shear MFC (N/mm^2)			Edge MFC (N/mm)		
K_{tc}	K_{rc}	K_{ac}	K_{te}	K_{re}	K_{ae}
538.127	185.967	–691.297	11.253	6.991	–32.971

3. 2. Verification of MF model

The measured and predicted MFs were described in **Fig. 8**. It is clear that the tendencies of the predicted MFs and the experimental MFs are quite close to each other. However, the values of the predicted and experimental peaks of MFs are still quite different. This difference can be explained by the fact that there are many parameters that have not been included in the MF models in this study such as vibrations, heat, friction, etc. So, the proposed models of milling forces from this study can be used to predict the cutting forces in face milling processes using square inserts. Besides, the proposed equations of cutting force coefficients also can be applied to determine the milling force coefficients in face milling process using square inserts.

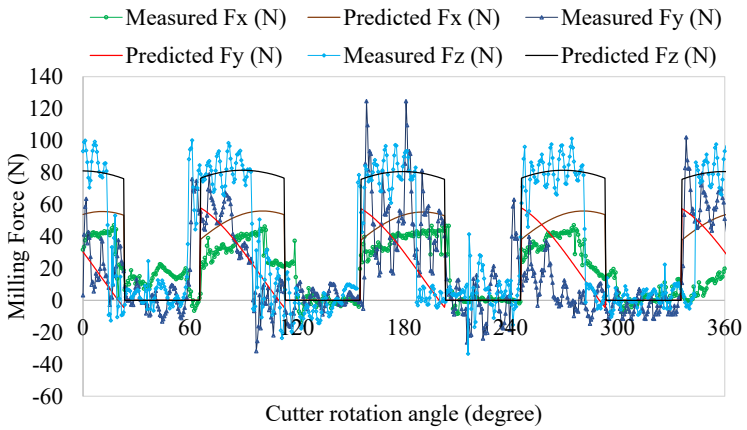

Fig. 8. Verification of MF model

3. 3. Limitations of the study and future directions

Although the cutting force model and cutting force coefficient have been determined through a combination of theoretical and experimental methods in this study, the research still has the limitations as listed below.

– in theory, the cutting force model in this study only focuses on the static models, so this proposed model is only suitable for application when machining with quite small values of speed;

– many factors have not been mentioned in this study such as the dynamic structure of the technological system, temperature, tool wear, etc. These issues are also the cause of the difference between the predicted cutting forces and the measured ones as mentioned in the results and discussion section of this study. In fact, all these factors influence on the cutting force during machining processes.

In order to complete the theoretical system relative to this study, further research directions are proposed including the following issues:

– develop the cutting force model from static models to dynamic models to apply to many different machining conditions;

– add the influence factors such as the dynamic structure of the technological system, cutting heat, cutting tool wear, etc. into the cutting force model to improve the accuracy when using these models to predict cutting forces during machining processes.

4. Conclusions

The conclusions of this study have been drawn as following:

– in the face milling process of Al7075 using square inserts, the AMFs have been modeled as a linear regression of *ft* with high determination coefficients (larger than 95 %);

– MFCs have been determined including shear and edge MFCs. These values are the tangential shear MFC (K_{tc}) of 538.127 N/mm^2, radial shear MFC (K_{rc}) of 185.967 N/mm^2, axial shear MFC (K_{ac}) of –691.297 N/mm^2, tangential edge MFC (K_{te}) of 11.253 N/mm, radial edge MFC (K_{re}) of 6.991 N/mm, and axial edge MFC (K_{ae}) of –32.971 N/mm;

– the MF models have been successfully verified by comparing the measured and predicted MFs in face milling process of Aluminum alloy Al7075. These cutting models and prediction method of cutting force coefficients in this study can be used to predict the cutting force coefficients and cutting forces in other milling types and other pairs of cutting tool and workpiece material as well.

Conflict of interest

The authors declare that they have no conflict of interest in relation to this research, whether financial, personal, authorship or otherwise, that could affect the research and its results presented in this paper.

Financing

The study was performed without financial support from any sources.

Data availability

The manuscript has no associated data.

Use of artificial intelligence

The authors confirm that they did not use artificial intelligence technologies when creating the current work.

Acknowledgements

The authors thank the support from Hanoi University for the measurement system in the experimental process.

References

[1] Wan, M., Lu, M.-S., Zhang, W.-H., Yang, Y. (2012). A new ternary-mechanism model for the prediction of cutting forces in flat end milling. International Journal of Machine Tools and Manufacture, 57, 34–45. https://doi.org/10.1016/j.ijmachtools.2012.02.003

[2] Nazma Sultana, Mst., Ranjan Dhar, N. (2023). Milling force modelling with high-pressure cooling strategy: An integrated analytical approach. Materials Today: Proceedings. https://doi.org/10.1016/j.matpr.2023.04.693

[3] Ding, P., Huang, X., Miao, X., Zhang, X., Li, Y., Wang, C. (2023). Mechanistic model and probability characteristics of micro-milling force with a new parameter identification method. Proceedings of the Institution of Mechanical Engineers, Part B: Journal of Engineering Manufacture, 238 (1-2), 199–213. https://doi.org/10.1177/09544054221149330

[4] Merchant, M. E. (1945). Mechanics of the Metal Cutting Process. I. Orthogonal Cutting and a Type 2 Chip. Journal of Applied Physics, 16 (5), 267–275. https://doi.org/10.1063/1.1707586

[5] Chen, Y., Lu, J., Deng, Q., Ma, J., Liao, X. (2022). Modeling study of milling force considering tool runout at different types of radial cutting depth. Journal of Manufacturing Processes, 76, 486–503. https://doi.org/10.1016/j.jmapro.2022.02.037

[6] Lazoglu, I. (2014). A New Identification Method of Specific Cutting Coefficients for Ball End Milling. Procedia CIRP, 14, 182–187. https://doi.org/10.1016/j.procir.2014.03.059

[7] Hoang, D. T., Nguyen, N.-T., Tran, Q. D., Nguyen, T. V. (2019). Cutting Forces and Surface Roughness in Face-Milling of SKD61 Hard Steel. Strojniški Vestnik – Journal of Mechanical Engineering, 65 (6), 375–385. https://doi.org/10.5545/sv-jme.2019.6057

[8] Sonawane, H. A., Joshi, S. S. (2010). Analytical modeling of chip geometry and cutting forces in helical ball end milling of superalloy Inconel 718. CIRP Journal of Manufacturing Science and Technology, 3 (3), 204–217. https://doi.org/10.1016/j.cirpj.2010.11.003

[9] Nguyen, N.-T. (2021). A development method of cutting force coefficients in face milling process using parallelogram insert. EUREKA: Physics and Engineering, 5, 36–52. https://doi.org/10.21303/2461-4262.2021.001890

[10] Ghorbani, H., Moetakef-Imani, B. (2015). Specific cutting force and cutting condition interaction modeling for round insert face milling operation. The International Journal of Advanced Manufacturing Technology, 84, 1705–1715. https://doi.org/10.1007/s00170-015-7985-2

[11] Andersson, C., Andersson, M., Ståhl, J.-E. (2011). Experimental studies of cutting force variation in face milling. International Journal of Machine Tools and Manufacture, 51 (1), 67–76. https://doi.org/10.1016/j.ijmachtools.2010.09.004

Received date 22.12.2023
Accepted date 14.04.2024
Published date 22.07.2024

How to cite: *Nguyen, N.-T., Xuan, H. L., Thinh, H. X., Nguyen, V.-H., Nguyen, H.-H. (2024). Modeling of milling forces in facing process of aluminum alloy Al7075 using the square inserts. EUREKA: Physics and Engineering, 4, 101–112. https://doi.org/10.21303/2461-4262.2024.003209*